Chapter 3

Efficient Evolution of Excitons into Charge Transfer States

3.0.1 ABSTRACT

Using first-principles molecular dynamics, we predict the reaction coordinate and mechanism of the first charge-transfer step in the reaction center of photosynthetic bacteria in a model including the special pair (P) and closest relevant residues. In the ground state, a dynamic localization of the highest occupied orbital is found to be a defining characteristic of P. This feature is linked to the tuning of the orbital energy levels by the coupling with two collective low-frequency vibrational modes. After electronic excitation, one specific mode coherently couples to P^*, representing the reaction coordinate along which the excited state develops. This characteristic vibrational coordinate represents the rotation of an axial histidine (HisM202), which selectively lowers the energy of one (P_M) of the two bacteriochlorophylls in P. This leads to an efficient and coherent evolution of $P_L^+P_M^-$ charge-transfer character, as the precursor of the full charge separated state $P^+B_A^-$.

Parts of this chapter were published in:
T. J. Eisenmayer, H. J. M. de Groot, E. van de Wetering, J. Neugebauer, F. Buda, "Mechanism and Reaction Coordinate of Directional Charge Separation in Bacterial Reaction Centers", *Journal of Physical Chemistry Letters*, **2012**, 3, pp 694-697.
DOI: 10.1021/jz201695p

3.1 Introduction

In the pseudo-symmetric architecture of photosynthetic reaction centers (RCs), charge separation occurs preferentially along one (A) of two cofactor branches. Numerous experiments find vibrational modes in the region 100-150 cm^{-1} that coherently couple to the initial photo-excited state of the special pair (P^*) [1-4].

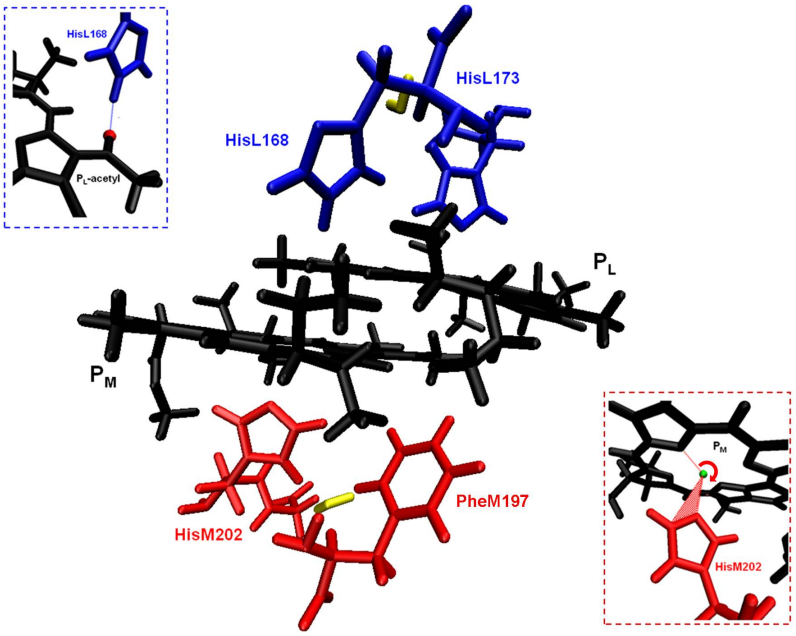

Figure 3.1: Model of the special pair and direct surroundings, including the axially coordinated histidines HisL173, HisM202, the water molecules in their vicinity, and the residues HisL168 and PheM197. The protein environment mechanical constraints are ensured by fixing the tails of the histidines, the phenylene, and the truncated phytyl chains. Left top: hydrogen bond between HisL168 and the acetyl oxygen of the P_L dimer half. Right bottom: dihedral angle of the histidine ring of HisM202 with respect to the Mg-N$_\tau$ coordination axis.

On a 3 ps time scale the primary electron donor is oxidized and an accessory bacteriochlorophyll (B_A) is reduced [5]. Stark experiments find an internal charge transfer (CT) character state $P_L^+P_M^-$ to have strong influence on P^* [6]. The ground-state electron density distribution of

P and of the radical cation $P^{\bullet+}$ is influenced by the immediate protein environment as indicated by solid-state NMR, ENDOR/EPR and density functional calculations [7,8]. The axial histidines are known to donate electron charge to bacteriochlorophyll chromophores both in reaction centers and light-harvesting complexes, and the acetyl groups conformation tunes the energy of the π-conjugated bacteriochlorophyll planes [9,10]. *Ab-initio* molecular dynamics (AIMD) simulations [11,12] have been performed at room temperature of a model including the special pair and the relevant closest protein environment (Figure 3.1). Long range interactions are not included in the model, but the chosen residues are thought to be sufficient to capture the most important effects for the local dynamics. Within this approach the dynamics of the nuclear coordinates is coupled to the corresponding electronic structure rearrangement calculated with density functional theory (DFT). This allows us to predict the reaction coordinate of coherent charge separation and the mechanism leading to the first charge transfer (CT) intermediate.

The AIMD simulations have been performed using the Car-Parrinello method [11,12] as implemented in the CPMD code [13]. The BLYP functional is used for the exchange-correlation energy [14]. The Kohn-Sham orbitals are expanded in a plane-wave basis set with a kinetic energy cutoff of 70 Ry and dispersion corrected atom-centered (DCACP) pseudopotentials [15] are used. For the excited state dynamics the restricted open-shell Kohn-Sham (ROKS) formalism [12] is applied. For the normal mode analysis and for single point calculations at selected snapshots along the AIMD trajectories I used the ADF code [16]. Also time dependent DFT (TDDFT) calculations have been performed using the ADF code for a selected set of configurations along the dynamical trajectories to evaluate the first excitation energies. Although TDDFT with standard GGA functionals suffers from the well known poor description of charge transfer character excitations, this analysis shows that the first excitation has a dominant HOMO to LUMO transition character. This finding justifies the use of the ROKS approach where only the HOMO to LUMO transition is taken into account to evaluate the excited state dynamics. Two AIMD ground state simulations have been performed of about 1 ps each starting from two sets of initial coordinates for our model taken from the X-ray crystallographic data of wild type [17] and R-26 mutant [18] *Rhodobacter Sphaeroides* reaction centers, respectively. The results presented in Figure 3.2 and 3.3 are obtained from the first trajectory using the wild type initial conditions. I verified that the trajectory generated from the R-26 mutant initial coordinates shows a pic-

ture consistent with the first trajectory. The ground state and excited state ROKS dynamics presented in Figure 3.4 are based on the R-26 initial conditions, while the inset of Figure 3.4 comes from the wild type model. The effect of long-range electrostatic interactions has been tested on a few snapshots along the trajectories by including a conductor like screening model (COSMO) using the ADF code with the same BLYP functional used in the AIMD simulations and a triple zeta with polarization basis set (TZP). A dielectric constant of 5 (a typical value in a protein environment) has been considered for this test. The relative energies of different configurations treated with and without the solvent model are well within 1 kcal/mol, thus confirming that the shape of the potential energy surface and therefore the force acting on the nuclei is not significantly modified by long range effects of the environment.

3.2 The Ground State

The ground state trajectories show that frontier orbital (HOMO-LUMO) localization is a dynamic characteristic of the special pair at room temperature (Figure 3.2).

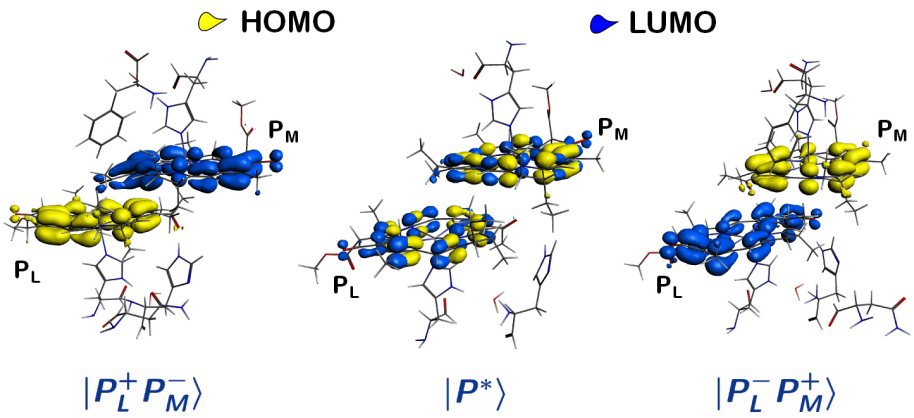

Figure 3.2: Frontier orbital localization for different snapshots along the trajectory. The HOMO fluctuates from localization on P_L (left) to a delocalized state (middle) to localization on P_M (right). Note that the LUMO shows the exact opposite behaviour, which leads to the CT character.

On a 1 ps timescale the HOMO fluctuates from complete localization on one dimer half to a delocalized state to complete localization on the other

dimer half. The LUMO shows the same dynamical behaviour with opposite phase; when the HOMO is localized on P_M the LUMO is localized on P_L and vice versa. This result can be interpreted by thermally induced orbital energy fluctuations of the two monomers: When the HOMO energy of P_L is lower than the HOMO energy of P_M, the HOMO of P shows an essentially monomeric character being localized entirely on P_L; when the orbital energies of the monomers are very similar, the HOMO is delocalized. HOMO-LUMO photoexcitation of P at specific geometries will thus yield an excited state with strong CT character. We find both $P_L^+P_M^-$ and $P_L^-P_M^+$ CT characters to be present at room temperature as well as a delocalized pure exciton state P^*. Comparing the relative HOMO-LUMO gap of $P_L^+P_M^-$ and $P_L^-P_M^+$ transitions it is shown, in agreement with Stark experiments [6], that $P_L^+P_M^-$ is the lowest energy CT transition of the P absorption band. The dynamic picture (Figure 3.2) and the occurrence of excitations with different character (P^*, $P_L^+P_M^-$ and $P_L^-P_M^+$) gives insight into the homogeneous broadening of the P absorption band and provides an explanation for its red shift at low temperatures. Going to low temperature the structural fluctuations are quenched as the system freezes gradually. This will eliminate the higher energy transitions in the absorption spectrum of P and leave the pure exciton transition with some $P_L^+P_M^-$ charge transfer character to dominate the band and red-shift the absorption maximum at low temperature. The HOMO is preferentially localized on P_L. Upon photo-oxidation of P the unpaired electron is assumed to be removed from the HOMO leading to a net spin density. Both NMR and ENDOR techniques measure a spin density distribution on bacterial RCs in the charge-separated radical cation $P^{\bullet+}$ state delocalized over the dimer with a 2:1 ration between P_L and P_M [19-20].

The thermal rearrangement of electron density over P opens the possibility to correlate electronic structure with distinct conformational dynamics, i.e. to find the normal modes of P that couple to orbital localization. Fourier transformation of the velocity autocorrelation function of the trajectories gives a vibrational density of states that shows two distinct maxima at low frequencies, $\sim$ 50 cm^{-1} and $\sim$ 100 cm^{-1} (Figure 3.3, grey shading in top graphs). To assign the peaks and resolve the appropriate conformational dynamics additional Fourier transforms of the autocorrelation function of different components of the model and of individual structural parameters (e.g. dihedral angles and bond distances) were performed. The lowest frequency peak at $\sim$ 50 cm^{-1} is well resolved in terms of the out-of-plane acetyl motion that couples strongly to the HisL168 imidazole ring dynamics

through hydrogen bonding interaction (see Figure 3.1, left top and Figure 3.3, blue lines). This is the characteristic vibrational coordinate of the mode, which is biased towards the P_L dimer half also absorbing at this frequency (see Figure 3.3, middle top inset, where the contribution of the two dimer halves is considered separately). To correlate the vibrational coordinate with the electronic structure, the energies of the HOMO and HOMO-1 along the trajectory are associated to either the P_L or P_M dimer half depending on their localization. The left bottom graph of Figure 3.3 shows the correlation between the P_L-HOMO energy (bars) and the hydrogen bond distance from the P_L-acetyl to the HisL168 with a computed Pearson correlation coefficient $\rho_c = 0.64$; at minimum distance, the hydrogen bond is strongest and stabilizes the P_L-HOMO energy.

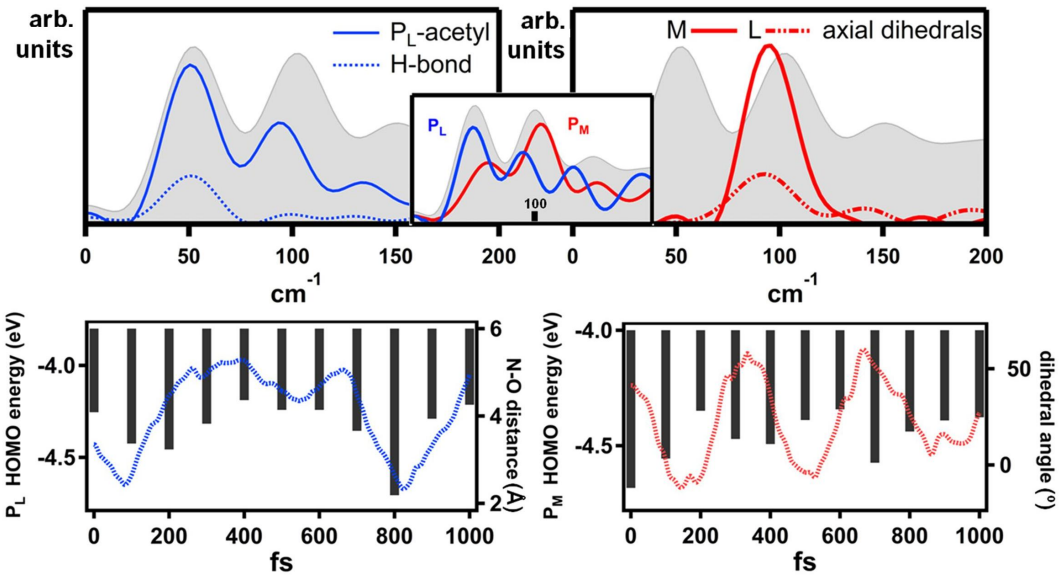

Figure 3.3: Total vibrational density of states (VDOS) obtained from the dynamical trajectory (grey shading top graphs). Blue lines in the top left represent conformational dynamics of the $\sim$ 50 cm^{-1} mode obtained from the time evolution of the hydrogen bond with HisL168 and of the P_L-acetyl group. The inset gives the VDOS for P_L in blue. The bottom left graph gives the hydrogen bond distance (blue line) with the P_L-HOMO energy (bars) in the time domain. Red lines represent conformational dynamics of the $\sim$ 100 cm^{-1} mode, top right graph gives the VDOS obtained from the axial histidine dihedrals and the inset the VDOS for P_M. The bottom right graph gives the HisM202 dihedral (red line) with the P_M-HOMO energy (bars) in the time domain.

In a separate calculation the Hessian matrix is diagonalized for the same model to analyze the normal modes. This calculation is performed using the Becke-Perdew functional. In agreement with the dynamical data the normal modes around $\sim$ 50 cm^{-1} are asymmetrically delocalized over P with an emphasis on P_L and with most of the amplitude along the characteristic vibrational coordinate represented by the concerted motion of the P_L-acetyl and the HisL168. In- and out-of-plane rotation of the acetyl group with respect to the bacteriochlorophyll macrocycle is well known to modulate the conjugated π-system [10]. The underlying structural cause for the $\sim$ 50 cm^{-1} mode to be dominated by the P_L-half acetyl group is that its symmetry-related counterpart on P_M acts as a sixth ligand to the Mg of P_L, inhibiting its free rotation. The average Mg-O^{acetyl} distances confirm this; the P_M acetyl group is $\sim$ 1 Å closer to the Mg on P_L 'locking' it into coordination.

Equally pronounced in the total vibrational density of states is a peak at $\sim$ 100 cm^{-1} that is mostly localized on the P_M half of the dimer (Figure 3.3; inset, red line). Analysis of the structural dynamics showed an intriguing anti-correlated rotation of the two axial histidines with respect to the coordination Mg-N$_\tau$ axis (illustrated by the inset in Figure 3.4; left top) expressed in terms of dihedral angles (see Figure 3.1 inset; right bottom). Calculations of covariance between the L- and M-side axial histidines ($\rho_c = -0.81$) confirm this behaviour yielding values a factor of 2 to 4 larger then the negative covariance between the L and M bacteriochlorophyll planes. From the Fourier analysis both dihedral angles are found to contribute to the $\sim$ 100 cm^{-1} mode, with the M-side dihedral showing larger amplitude (see Figure 3.3, top right, red lines). The normal mode analysis clearly confirms this picture; the modes around $\sim$ 100 cm^{-1} contain an anti-correlated rotation of the axial histidines with respect to the $Mg-N_\tau$ axis, the amplitude being larger on the M-side. In conclusion, the characteristic vibrational coordinate of the $\sim$ 100 cm^{-1} mode involves mostly the P_M dimer half and the axial rotation of the HisM202. The bottom right graph of figure 3.3 shows the dihedral angle of HisM202 (red line) with the energy of the P_M-HOMO (bars) along the trajectory. Minima at 0, 350 and 700 fs in the energy of the P_M-HOMO correspond to maxima in the dihedral angle revealing that these quantities are anti-correlated ($\rho_c = -0.50$). The ground state multidimensional configurational space along which the relative energies of P_L and P_M are modulated is thus essentially given by two collective coordinates with well defined frequencies ($\sim$ 50 cm^{-1} and $\sim$ 100 cm^{-1}). Displacements along these coordinates changes the localization

of the frontier orbitals.

3.3 The Excited State

To explore the dynamics in the excited state (P^*) a molecular dynamics simulation based on the restricted open-shell Kohn-Sham (ROKS) approach [12] has been performed starting from the previously equilibrated ground state trajectory. The use of ROKS is justified given the dominant HOMO-LUMO character of the excitation. By comparing the ground state and the ROKS trajectories a distinct conformational change induced by the photo-excitation is apparent. This is illustrated in figure 3.4, showing the dihedral angles of the rotation of the axial histidines around the Mg-N_τ axis. In the ground state a striking negative covariance between the rotations of the two histidines was found (see also the inset in Figure 3.4).

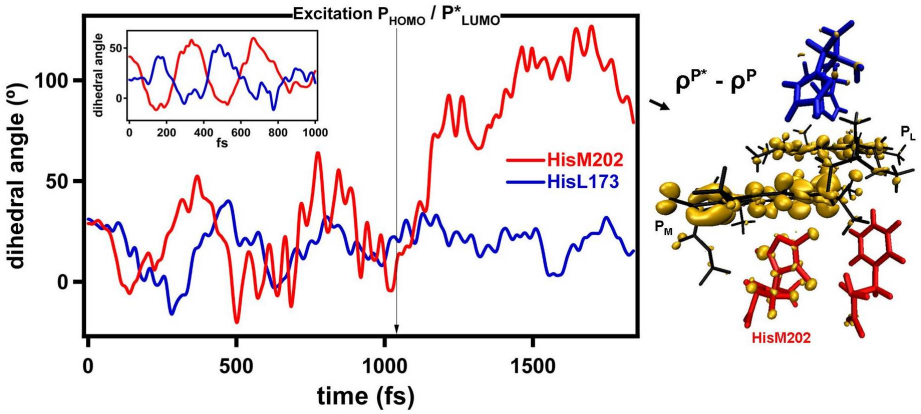

Figure 3.4: HisM202 (red line) and symmetry related HisL173 (blue line) dihedral angles representing the rotation of the histidine rings around the coordination $Mg - N_\tau$ axis as a function of time (see also Figure 3.1, right bottom). The arrow indicates the time step of the switch from ground state to excited state (ROKS) dynamics. In the inset for comparison the same structural parameters along a different ground state trajectory. The right figure shows the positive values of the difference between the P^* and P electron density ($\rho^{P^*} - \rho^P$) at the end of the ROKS dynamics.

After photo-excitation the dihedral angle of HisM202 (red line), that was found to be characteristic of the vibrational coordinate of the $\pm$ 100 cm^{-1}) mode, increases from an average of $\sim 25°$ in the ground state to $\sim 80°$ in

P^* and the negative covariance is lost. The vibrational coordinate of the $\pm$ 50 cm^{-1} mode is not affected upon photo-excitation. In conclusion, upon photo-excitation P couples selectively to the $\pm$ 100 cm^{-1} mode which I propose is the same mode seen in resonance Raman studies (96 cm^{-1}), [22] in femtosecond absorption spectroscopy (94 cm^{-1}) [3], and possibly hole-burning studies ($\sim$ 150 cm^{-1}) [4]. To check the effect of the dynamics on the evolution in the excited state and the electron density distribution the difference between the excited state and ground state electron density for selected snapshots along the ROKS dynamics is considered. In Figure 3.4 (right) the positive values of $\rho^{P^*} - \rho^P$ are plotted. Electron density moves from P_L to P_M and onto the HisM202 in agreement with experimental findings that P^* is dominated by a $P_L^+ P_M^-$ CT character [6,23].

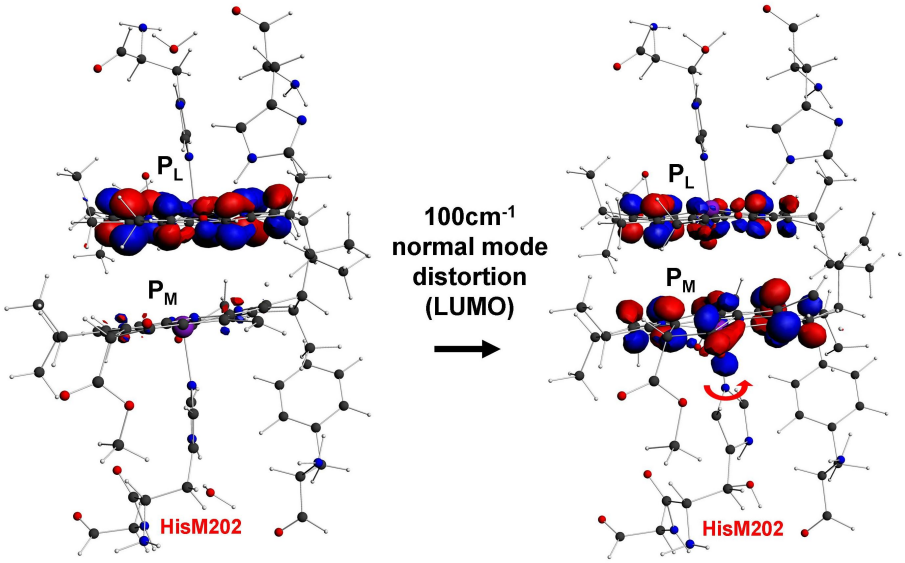

Figure 3.5: LUMO redistribution as a function of a displacement along the 100 cm^{-1} normal mode resulting in a rotation of the HisM202 around the coordination Mg-N$_\tau$ axis from 5° (left) to 50° (right).

To confirm that the excited state electron density redistribution is due to the coupling of the excited state with the discussed 100 cm^{-1} mode, I show in Figure 3.5 how the LUMO is redistributed by a displacement along this normal mode. The amplitude of the displacement is chosen such that the

HisM202 dihedral angle - representative of the rotation of the histidine around the coordination Mg-N_τ axis - increases from 5° to 50°. This confirms that the reaction coordinate, even starting from a $P_L^- P_M^+$ CT configuration, leads to a $P_L^+ P_M^-$ intermediate state through the coupling of P^* to the 100 cm^{-1} mode resulting in an increase of the dihedral angle and initiating a directional displacement of electron density. From the Moser-Dutton simplification, the donor-acceptor distance is the rate-defining variable in most biological electron-transfer reactions [24,25]. In the bacterial RC, where competing electron-transfer pathways have similar distances, the reaction coordinate - as identified in this work - displaces electron density asymmetrically, possibly increasing the electronic coupling with one (B_A) of the two accessory bacteriochlorophylls. Additional investigations with an extended model including the electron acceptor are needed to support this suggestion (see Chapter 4).

3.4 Conclusions

In conclusion, the ground state electron density is continuously redistributed by thermally excited low frequency collective modes ($\sim$ 50 cm^{-1} and $\sim$ 100 cm^{-1}) that tune the respective dimer halves energies and induce the thermal broadening of P. Upon photo-excitation the excited state P^* specifically couples to the $\sim$ 100 cm^{-1} mode that lowers the P_M dimer half energy and effectively modulates the barrier for charge separation allowing a coherent displacement of electron density towards a $P_L^+ P_M^-$ charge transfer intermediate. Thus, I have structurally characterized the nuclear motion that drives the efficient charge separation in bacterial reaction centers. Further nonadiabatic, excited state dynamics would be needed to directly observe the oscillatory evolution of charge transfer character in combination with, for example, two-dimensional electronic spectroscopy.

3.5 References

[1] Novoderezhkin, V.; Yakovlev, A.; van Grondelle, R.; Shuvalov, V. Coherent Nuclear and Electronic Dynamics in Primary Charge Separation in Photosynthetic Reaction Centers: A Redfield Theory Approach. J. Phys. Chem. B 2004, 108, 7445-7457.

[2] Vos, M. H.; Jones, M. R.; Hunter, C. N.; Breton, J.; Martin, J. L. Coherent Nuclear Dynamics at Room Temperature in Bacterial Reaction Centers. Proc. Natl. Acad. Sci. U.S. A. 1994, 91, 12701- 12705.

[3] Rischel, C.; Spiedel, D.; Ridge, J. P.; Jones, M. R.; Breton, J.; Lambry, J. C.; Martin, J. L. Low Frequency Vibrational Modes in Proteins: Changes Induced by Point-Mutations in the Protein- Cofactor Matrix of Bacterial Reaction Centers. Proc. Natl. Acad. Sci. U.S.A. 1998, 95, 12306-12311.

[4] Reddy, N. R. S.; Kolaczkowski, S. V.; Small, G. J. A Photoinduced Persistent Structural Transformation of the Special Pair of a Bacterial Reaction Center. Science 1993, 260, 68-71.

[5] Holzapfel, W.; Finkele, U.; Kaiser, W.; Oesterhelt, D.; Scheer, H.; Stilz, H. U.; Zinth, W. Initial Electron-Transfer in the Reaction Center from Rhodobacter Sphaeroides. Proc. Natl. Acad. Sci. U.S.A. 1990, 87, 5168-5172.

[6] Moore, L. J.; Zhou, H.; Boxer, S. G. Excited-State Electronic Asymmetry of the Special Pair in Photosynthetic Reaction Center Mutants: Absorption and Stark Spectroscopy. Biochemistry 1999, 38, 11949-11960.

[7] Daviso, E.; Prakash, S.; Alia, A; Gast, P.; Neugebauer, J.; Jeschke, G.; Matysik, J. The Electronic Structure of the Primary Electron Donor of Reaction Centers of Purple Bacteria at Atomic Resolution As Observed by Photo-CIDNP 13C NMR. Proc. Natl. Acad. Sci. U. S. A. 2009, 106, 22281-22286.

[8] Johnson, E. T.; Mu, F.; Nabedryk, E.; Williams, J. C.; Allen, J. P.; Lubitz, W.; Breton, J.; Parson, W. W. Electronic and Vibronic Coupling of the Special Pair of Bacteriochlorophylls in Photosynthetic Reaction Centers from Wild-Type and Mutant Strains of Rhodobacter Sphaeroides. J. Phys. Chem. B 2002, 106, 11859-11869.

[9] Alia, Wawrzyniak, P. K.; Janssen, G. J.; Buda, F.; Matysik, J.; de Groot, H. J. M. Differential Charge Polarization of Axial Histidines in Bacterial Reaction Centers Balances the Asymmetry of the Special Pair. J. Am. Chem. Soc. 2009, 131, 9626-9627.

[10] Wawrzyniak, P. K.; Beerepoot, M. T. P.; de Groot, H. J. M.; Buda, F. Acetyl Group Orientation Modulates the Electronic Ground- State Asymmetry of the Special Pair in Purple Bacterial Reaction Centers. Phys. Chem. Chem. Phys. 2011, 13, 10270-10279.

[11] Car, R.; Parrinello, M. Unified Approach for Molecular Dynamics and Density-Functional Theory. Phys. Rev. Lett. 1985, 55, 2471-2474.

[12] Marx, D.; Hütter, J. Ab Initio Molecular Dynamics: Basic Theory and Advanced Methods; Cambridge University Press: Cambridge, U.K., 2009.

[13] CPMD v3.11.1, Copyright IBM Corp, 1990-2008; Copyright MPI für Festkörperforschung Stuttgart, 1997-2001; http://www.cpmd.org/.

[14] a) A.D. Becke, Phys. Rev. A 1988, 38, 3096; b) C.T. Lee, W.T. Yang, R.G. Parr, Phys. Rev. B 1988, 37, 785.

[15] a) O.A. von Lilienfeld, I. Tavernelli, U. Röthlisberger, D. Sebastiani, Phys. Rev. Lett.2004, 93, 153004; b) O.A. von Lilienfeld, I. Tavernelli, U. Röthlisberger, D. Sebastiani, Phys. Rev. B 2005, 71, 195119.

[16] ADF2010, SCM, Theoretical Chemistry, Vrije Universiteit, Amsterdam, The Netherlands, http:// www.scm.com/.

[17] U. Ermler, G. Fritzsch, S.K. Buchanant, H. Michel, Structure 1994, 2, 925-936.

[18] M.H. Stowell, T.M. McPhillips, D.C. Rees, S.M. Soltis, E. Abresch, G. Feher, Science1997, 276, 812-816.

[19] E. Daviso, S. Prakash, A. Alia, P, Gast, J. Neugebauer, G. Jeschke, J. Matysik, Proc. Natl. Acad. Sci. U. S. A. 2009, 106, 22281-22286.

[20] E. T. Johnson, F. Mu, E. Nabedryk, J.C. Williams, J.P. Allen, W. Lubitz, J. Phys. Chem. B 2002, 106, 11859-11869.

[21] Cohen Stuart, T.; van Grondelle, R. Multipulse Spectroscopy on the Wild-Type and YM210W Bacterial Reaction Centre Uncovers a New Intermediate State in the Special Pair Excited State. Chem. Phys. Lett. 2009, 474, 352-356.

[22] Cherepy, N. J.; Shreve, A. P.; Moore, L. J.; Boxer, S. G.; Mathies, R. A. Temperature Dependence of the Qy Resonance Raman Spectra of Bacteriochlorophylls, the Primary Electron Donor, and Bacteriopheophytins in the Bacterial Photosynthetic Reaction Center. Biochemistry 1997, 36, 8559-8566.

[23] Shuvalov, V.; Yakovlev, A. Coupling of Nuclear Wavepacket Motion and Charge Separation in Bacterial Reaction Centers. FEBS Lett. 2003, 540, 26-34.

[24] Moser, C. C.; Keske, J. M.; Warncke, K; Farid, R. S.; Dutton, L. P. Nature of Biological Electron Transfer. Nature 1992, 355, 796-802.

[25] Creighton, S.; Hwang, J. K.; Warshel, A; Parson, W. W.; Norris, J. Simulating the Dynamics of the Primary Charge Separation Process in Bacterial Photosynthesis. Biochemistry 1988, 27, 774-781.